Unusual Mott transition associated with charge-order melting in $BiNiO_3$ under pressure

I. Leonov,[1,2] A. S. Belozerov,[1,3] and S. L. Skornyakov[1,3]

[1] *M. N. Miheev Institute of Metal Physics, Russian Academy of Sciences, 620108 Yekaterinburg, Russia*
[2] *Materials Modeling and Development Laboratory, National University of Science and Technology 'MISiS', 119049 Moscow, Russia*
[3] *Ural Federal University, 620002 Yekaterinburg, Russia*

We study the electronic structure, magnetic state, and phase stability of paramagnetic $BiNiO_3$ near a pressure-induced Mott insulator-to-metal transition (MIT) by employing a combination of density functional and dynamical mean-field theory. We obtain that $BiNiO_3$ exhibits an anomalous negative-charge-transfer insulating state, characterized by charge disproportionation of the Bi $6s$ states, with Ni^{2+} ions. Upon a compression of the lattice volume by ∼4.8%, $BiNiO_3$ is found to make a Mott MIT, accompanied by the change of crystal structure from triclinic $P\bar{1}$ to orthorhombic $Pbnm$. The pressure-induced MIT is associated with the melting of charge disproportionation of the Bi ions, caused by a charge transfer between the Bi $6s$ and O $2p$ states. The Ni sites remain to be Ni^{2+} across the MIT, which is incompatible with the valence-skipping Ni^{2+}/Ni^{3+} model. Our results suggest that the pressure-induced change of the crystal structure drives the MIT in $BiNiO_3$.

The Mott metal-insulator transition driven by correlation effects has been an outstanding problem in condensed matter physics over many decades [1]. In recent years, increasing attention has been drawn to the rare earth nickelate perovskites $R\mathrm{NiO_3}$ (R = rare earth, R^{3+}) with a high oxidation state of nickel, Ni^{3+} $3d^7$ [2–4]. $R\mathrm{NiO_3}$ compounds (except for $LaNiO_3$) exhibit a sharp metal-insulator transition (MIT) upon cooling below T_{MIT} [5]. The phase transition is accompanied by a structural transformation from an orthorhombic ($Pbnm$, $GdFeO_3$-type) to monoclinic ($P2_1/n$) crystal structure, with a cooperative breathing distortion of NiO_6 octahedra [5].

Based on the Ni-O bond lengths analysis and X-ray absorption spectroscopy, a partial $Ni^{(3\pm\delta)+}$ charge disproportionation of Ni ions was proposed to occur in the insulating $R\mathrm{NiO_3}$ phases [5, 6]. By contrast, further electronic structure calculations explain the insulating state of $R\mathrm{NiO_3}$ in terms of bond disproportionation, with alternating Ni ions which (nearly) adopt a Ni^{2+} $3d^8$ (Ni^{2+} ions with local moments) and $3d^8\underline{L}^2$ (nonmagnetic spin-singlet) electronic configuration ($\underline{L}$ denotes a hole in the O $2p$ band) [3, 8, 8]. The transition temperature T_{MIT} is strongly related to the degree of structural distortion of $R\mathrm{NiO_3}$, determined by the size of R-ions. With decrease of the R-ionic radius, the Ni-O-Ni bond angle, which determines the degree of overlapping of the Ni $3d$ and O $2p$ orbitals (and hence the Ni $3d$ bandwidth), becomes smaller and T_{MIT} is increased. In accord with this, the least distorted $LaNiO_3$ is found to be a correlated metal [5, 9]. In this context, the replacement of La^{3+} with a larger ion, such as Bi^{3+}, should in principle result in a metal with (nearly) cubic perovskite structure. By contrast, $BiNiO_3$ has been found to be an insulator with a highly distorted perovskite structure (triclinic, $P\bar{1}$) and unusual valence ordering of the A-site Bi ions [1]. In particular, based on X-ray and neutron diffraction, it was proposed that Ni ions adopt a Ni^{2+} state, with an electronic configuration $Bi^{3+}_{0.5}Bi^{5+}_{0.5}Ni^{2+}O_3$ [1, 11, 12].

$BiNiO_3$ is known due to its colossal negative thermal expansion across the pressure-induced MIT, as suggested caused by a Bi/Ni charge transfer [13]. Under ambient conditions, $BiNiO_3$ crystallizes in a triclinic perovskite crystal structure (space group $P\bar{1}$, a subgroup of $P2_1/n$) with two inequivalent Bi and four Ni sites [11] (see Supplementary Fig. S1 [14] and Ref. [12] therein). It is an insulator with an energy gap of 0.68 eV [1]. Below the Néel temperature of $T_{\mathrm{N}} \sim 300$ K, $BiNiO_3$ is a G-type antiferromagnet with a near-antiferromagnetic alignment of Ni^{2+} $S = 1$ spins, implying a predominant role of the antiferromagnetic Ni-O-Ni superexchange [1, 12, 16]. Moreover, similarly to the small R-ions $R\mathrm{NiO_3}$ the (charge-disproportionated) paramagnetic insulating phase of $BiNiO_3$ extends well above T_{N}, implying the crucial importance of correlation effects [3, 8, 17]. $BiNiO_3$ shows a Mott insulator-to-metal phase transition (in the paramagnetic phase) under pressure (above ∼4 GPa) or upon substitution of the A-site Bi ions with La [10, 18]. In close similarity to $R\mathrm{NiO_3}$, the MIT is accompanied by the change of crystal structure from the triclinic $P\bar{1}$ (insulating) to orthorhombic $GdFeO_3$-type $Pbnm$ (metallic) phase, with a volume collapse of ∼3% and melting of charge disproportionation (Ni and Bi sites are equivalent in the $Pbnm$ structure of $BiNiO_3$). Based on the powder X-ray absorption and neutron diffraction, it was proposed that the melting of charge disproportionation leads to a charge transfer from Ni^{2+} to Bi^{3+}, so that the electronic state of the $Pbnm$ metallic phase can be described as $Bi^{3+}Ni^{3+}O_3$ [11, 20]. This valence distribution however is in odd with photoemission spectroscopy results for $Pbnm$ $BiNiO_3$ that reveal that the nickel valence is far from being Ni^{3+} [10].

The electronic properties of $BiNiO_3$ have recently been calculated using band-structure methods supplemented with the on-site Coulomb correlations for the Ni $3d$ states within density-functional theory (DFT)+U [21] and dynamical mean-field theory (DMFT) [22] methods [23].

However, these studies have mostly been focused on the valence skipping model, with a valence transition between the charge-ordered insulating $[Bi^{3+}_{0.5}Bi^{5+}_{0.5}][Ni^{2+}]$ and the uniform metallic $[Bi^{3+}][Ni^{3+}]$ state, assuming a long-range magnetic ordering. In fact, however, the MIT transition in $BiNiO_3$ is known to occur in the *paramagnetic* state, implying the importance of electronic correlations. Moreover, a recent electronic structure study of $BiNiO_3$ using DFT and slave rotor methods suggests that $BiNiO_3$ is a self-doped Mott insulator [24].

In this paper, we explore the evolution of the electronic structure, magnetic state, and phase stability of paramagnetic $BiNiO_3$ near the pressure-induced Mott MIT. We employ a fully self-consistent in charge density DFT+DMFT approach [2] implemented with plane-wave pseudopotentials [3, 4] which makes it possible to capture all generic aspects of the interplay between the electronic correlations, magnetic states, and crystal structure of $BiNiO_3$ near the Mott MIT [28]. The DFT+DMFT calculations explicitly include the Bi $6s$, O $2p$, and Ni $3d$ valence states, by constructing a basis set of atomic-centered Wannier functions within the energy window spanned by the *s-p-d* band complex [29]. This allows us to take into account a charge transfer between the Bi $6s$, O $2p$, and Ni $3d$ states, accompanied by the strong on-site Coulomb correlations of the Ni $3d$ electrons. We use the continuous-time hybridization-expansion (segment) quantum Monte-Carlo algorithm in order to solve the realistic many-body problem [7]. We take the average Hubbard $U = 6$ eV and Hund's exchange $J = 0.95$ eV as estimated previously for RNiO$_3$ [8, 9]. We use the fully localized double-counting correction, evaluated from the self-consistently determined local occupations, to account for the electronic interactions already described by DFT.

In Fig. 1 we display our DFT+DMFT results for the phase equilibrium and local magnetic moments of Ni ions of paramagnetic $BiNiO_3$. In these calculations, we adopt the crystal structure data for the ambient pressure triclinic $P\bar{1}$ and high-pressure orthorhombic $Pbnm$ structures (taken at a pressure of ∼7.7 GPa) from experiment [11], and evaluate the DFT+DMFT total energies as a function of lattice volume. Overall, our results for the electronic structure and lattice properties of $BiNiO_3$ agree well with experimental data [1, 10–13]. In particular, the triclinic $P\bar{1}$ phase is found to be thermodynamically stable at ambient pressure, with a total-energy difference between the ambient-pressure and high-pressure phases of ∼160 meV/f.u.. The calculated equilibrium lattice volume $V_0 = 248.8$ Å^3 and bulk modulus $K_0 = 149$ GPa ($K' \equiv dK/dP$ is fixed to $K' = 4$). Interestingly, all the Ni sites (the insulating $P\bar{1}$ phase has four inequivalent Ni sites) are nearly equivalent and are in the Ni^{2+} state. The Ni^{2+} state is also confirmed by the eigenvalues analysis of the reduced Ni $3d$ density matrix, which suggests that the Ni ions are in the $\sqrt{0.63}|d^8\rangle + \sqrt{0.32}|d^9\rangle$ state (all the rest contributions are below 0.05). Moreover, the calculated local (instantaneous) magnetic moment $\sqrt{\langle \hat{m}_z^2 \rangle} \simeq 1.67\,\mu_B$, agrees with the high-spin $S = 1$ state of the Ni^{2+} ions.

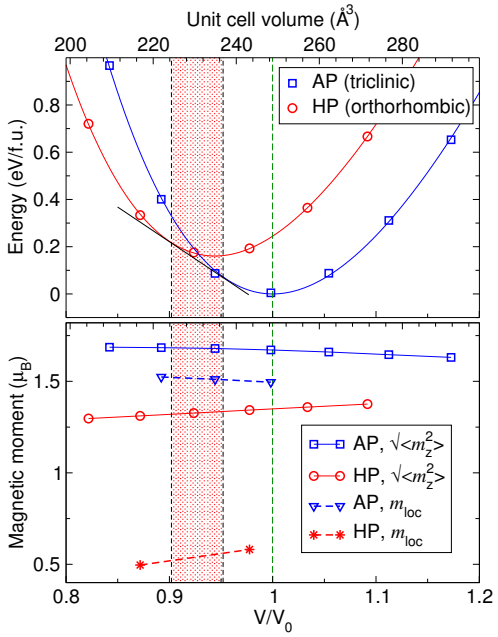

FIG. 1: (Color online) Total energy (top) and local magnetic moments (bottom) of paramagnetic $BiNiO_3$ obtained by DFT+DMFT for the ambient-pressure $P\bar{1}$ (AP) and high-pressure $Pbnm$ (HP) phases as a function of the unit cell volume at a temperature $T = 387$ K.

Our calculations for the insulating $P\bar{1}$ phase of $BiNiO_3$ give a self-doped Mott insulator [31] with an energy gap of ∼0.3 eV (see the left panel of Fig. 2), in agreement with the resistivity and photoemission experiments [1, 10] (see also Supplementary Fig. S3). In particular, the energy gap lies between the occupied and unoccupied Ni e_g states, strongly mixed with the O $2p$ and the empty Bi2 $6s$ states (the Bi1 $6s$ states are fully occupied). The O $2p$ states are about -3.6 eV below the Fermi level, but have a substantial contribution both above and below E_F. The latter is due to the strongly covalent B $6s$–O $2p$ bonding, suggesting creation of a ligand hole caused by a charge transfer between Bi $6s$ and O $2p$. While the occupied Bi1 and Bi2 $6s$ states are seen to be localized deep below E_F, at about -10 eV, the empty Bi2 $6s$ states appear right at the bottom of the conduction band, with a sharp resonant peak at ∼0.4 eV. The top of the valence band has a mixed Ni $3d$ and O $2p$ character, with a resonant peak in the filled e_g bands located at about -0.4 eV below the Fermi level, which can be ascribed to the formation of a Zhang-Rice bound state [32].

Our result for the insulating $P\bar{1}$ phase is characterized by a remarkable charge disproportionation of the Bi $6s$ states (due to the appearance of two different Bi sites with sufficiently different oxygen environment in the insulating phase). In fact, while the Bi1 $6s$ states are almost completely occupied, the Bi2 $6s$ Wannier occupancy is only about 1.56. This implies a

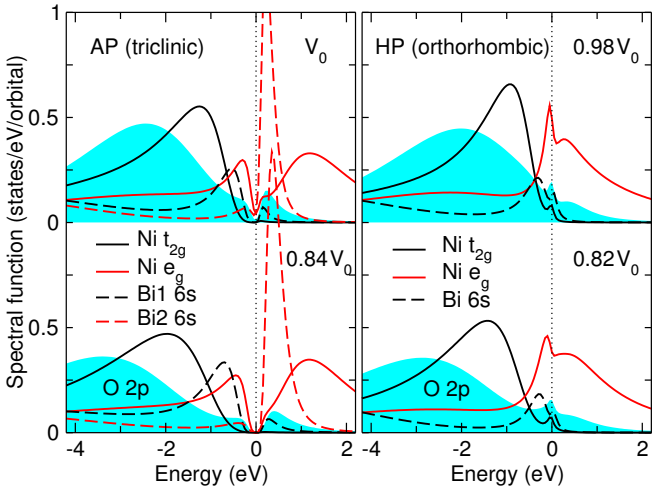

FIG. 2: (Color online) Orbitally-resolved spectral functions of $BiNiO_3$ calculated within DFT+DMFT using the maximum entropy method for the ambient-pressure $P\bar{1}$ (left panel) and high-pressure $Pbnm$ (right panel) structures for different unit cell volumes at a temperature $T = 387$ K.

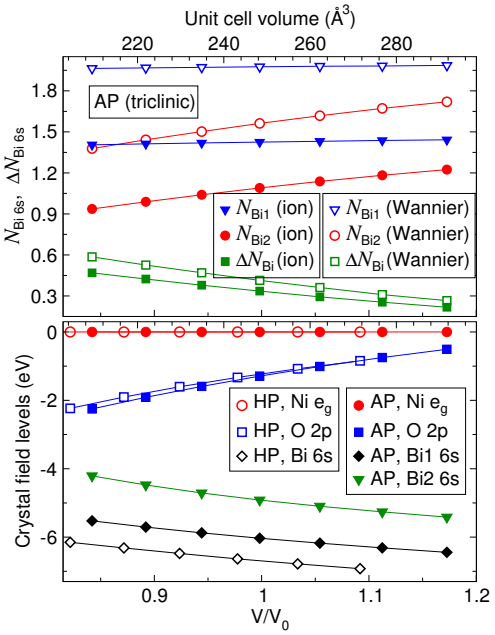

FIG. 3: (Color online) Bi $6s$ occupations for the ambient-pressure (AP) $P\bar{1}$ phase of $BiNiO_3$ calculated by DFT+DMFT as a function of lattice volume (top). $\Delta N_{\rm Bi}$ denotes the corresponding Bi $6s$ charge disproportionation ($\Delta N_{\rm Bi} = N_{\rm Bi1} - N_{\rm Bi2}$). Bottom: the Ni e_g and O $2p$ crystal field levels for the AP and high-pressure $Pbnm$ $BiNiO_3$ [35].

charge difference of $\Delta N_{\text{Bi-}6s} \sim 0.42$, i.e., it is about 21% of the ideal Bi^{3+}-Bi^{5+} value. Interestingly, the corresponding Bi $6s$ charge difference is in agreement with a charge disproportionation of ∼0.2 (i.e., of ∼20% of the ideal valence skipping) found in the low-temperature charge-ordered phases of the mixed-valent oxides, such as Fe_3O_4 [33], and of ∼0.2-0.3 charge disproportionation of the Ni ions in $R NiO_3$ [5]. Moreover, previous estimates for the bond-disproportionated insulating phases of the bismuth perovskites $BaBiO_3$ and $SrBiO_3$ show a small charge disproportionation between the Bi ions of ∼0.3 [34]. We also verified our result for $\Delta N_{\text{Bi-}6s}$ by calculating the corresponding charge difference within the Bi-ion radius of 1.31 Å, a typical value for the Bi^{3+} ion. Nevertheless, we find that the result is robust, with $\Delta N_{\text{Bi-}6s} \sim 0.34$. While all the Ni's are in the Ni^{2+} state (and, as we will show below, the Ni^{2+} state remains stable above the MIT in the metallic $Pbnm$ phase) this suggests the stabilization of the charge disproportionated $\text{Bi}1^{3+}_{0.5}(\text{Bi}2^{(3+\delta)+}\underline{L}^{2-\delta})_{0.5}$ valence configuration in the insulating $P\bar{1}$ phase of $BiNiO_3$. We argue that the obtained valence configuration can be rationalized as being intermediate between the two limits: the pure valence skipping Bi^{3+}-Bi^{5+} and the Bi-O bond disproportionation Bi^{3+}-$[Bi^{3+}\underline{L}^2]$ models.

Interestingly, the energy gap of the triclinic $BiNiO_3$ phase is seen to increase upon (an uniform) compression (while decreasing and even closing upon expansion) of the unit cell volume (see the lower panel of Fig. 2). This counter-intuitive change of the energy gap value in a Mott insulator is accompanied by a remarkable increase of charge disproportionation of the Bi ions (under pressure), suggesting the importance of a Bi $6s$-O $2p$ charge transfer. In particular, our results show that the Bi $6s$ charge disproportionation becomes larger in the $P\bar{1}$ crystal structure of $BiNiO_3$ upon decrease of the lattice volume (see Fig. 3). Upon compression, the Bi2 $6s$ orbital occupation gradually decreases, whereas the Bi1 $6s$ states are fully occupied, with a nearly constant occupation $N_{\text{Bi1-}6s} \sim 1.97$. In addition, our DFT+DMFT calculations using different Hubbard U values ($U = 5$ eV and 8 eV) show that the energy gap increases upon increasing of U, in agreement with the behavior of a Mott insulator. Interestingly, the Bi $6s$ charge disproportionation becomes larger for the larger U values, by ∼5% upon increasing of the U value from $U = 6$ eV to 8 eV.

This behavior is consistent with the change of the crystal field levels of the Ni e_g, O $2p$, and Bi $6s$ states under pressure (see Fig. 3). In fact, the O $2p$ levels are found to shift deep below the Ni e_g states under pressure, whereas the Bi $6s$ states go up in energy. The change of the O $2p$ and Bi $6s$ crystal field levels leads to the enhancement of the Bi $6s$-O $2p$ hybridization under pressure, supporting the hybridization-switching mechanism proposed by Paul *et al.* [24]. Our results suggest that the $P\bar{1}$-structured $BiNiO_3$ is an *unconventional* Mott insulator in which the correlated insulating state is in much respect controlled by an s-p level splitting between the uncorrelated A-site Bi $6s$ and ligand O $2p$ states.

Upon further compression the $P\bar{1}$-structured $BiNiO_3$ becomes metallic below $\sim 0.5\,V_0$, with the (instantaneous) local moment of $\sim 1.36\,\mu_{\rm B}$. The MIT is accompanied with a collapse of local moments due to delocalization of the Ni $3d$ electrons, as seen from the be-

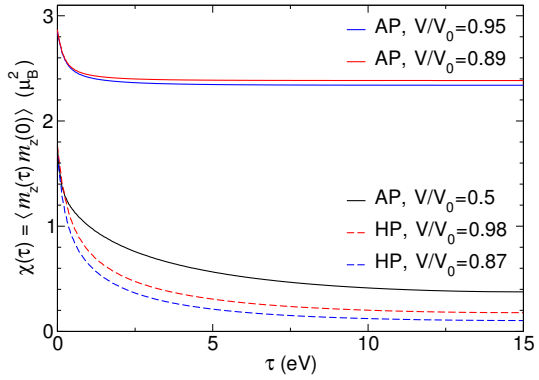

FIG. 4: (Color online) Local spin correlation function $\chi(\tau) = \langle \hat{m}_z(\tau)\hat{m}_z(0)\rangle$ of the Ni $3d$ states calculated by DFT+DMFT for the ambient-pressure $P\bar{1}$ (AP) and the high-pressure $Pbnm$ (HP) structures of $BiNiO_3$ for different volumes.

havior of local spin susceptibility $\chi(\tau) = \langle \hat{m}_z(\tau)\hat{m}_z(0)\rangle$ (see Fig. 4). In fact, $\chi(\tau)$ is seen to decay fast with the imaginary time τ. In agreement with this, the fluctuating moment is only of $\sim$0.75 μ_B (evaluated as $m_{loc} = [T\int_0^{1/T}\chi(\tau)d\tau]^{1/2}$), that differs sufficiently from the instantaneous moment. While the Bi $6s$ charge disproportionation is large in the highly-compressed metallic $P\bar{1}$ phase, $\Delta N_{\text{Bi-}6s} \sim 1.04$, this suggests that the Bi $6s$ charge ordering alone cannot explain the insulating state of $BiNiO_3$. In agreement with this, our results for structural optimization of the $P\bar{1}$ phase within nonmagnetic DFT give a metal with no evidence for the Bi $6s$ charge disproportionation (all the Bi sites are found to have nearly same oxygen environment), implying the crucial importance of strong localization of the Ni $3d$ electrons due to correlation effects [3].

Most importantly, our DFT+DMFT results provide a clear evidence that $BiNiO_3$ undergoes a structural transition from the triclinic insulating $P\bar{1}$ to orthorhombic metallic $Pbnm$ structure below $\sim 0.95\,V_0$ (above 8 GPa), in agreement with experiment [11–13]. We found that the transition pressure depends very sensitively on the choice of the Hubbard U value, with $P_c \simeq 1$ GPa and 15 GPa for $U = 5$ eV and 8 eV, respectively. The calculated bulk modulus ($U = 6$ eV) is $K_0 \sim 143$ GPa, i.e., K_0 is found to decrease by $\sim$4% upon the MIT into the metallic state. The latter is rather uncommon for a Mott MIT, indicating the importance of lattice effects at the MIT in $BiNiO_3$ [3].

The $Pbnm$ phase of $BiNiO_3$ is a correlated metal, characterized by a Fermi-liquid-like behavior with a weak damping of quasiparticles at the Fermi energy and by a substantial mass renormalization of $\frac{m^*}{m} \sim 2.5$ of the Ni e_g bands. The Ni e_g states show a quasiparticle peak at the Fermi level, with the upper Hubbard band at $\sim$ 1.0 eV (see Fig. 2 and Supplementary Fig. S3). The calculated Ni-ion local magnetic moment of $1.3\,\mu_B$ differs sufficiently from the fluctuating one $\sim 0.5\,\mu_B$, implying delocalization of the Ni $3d$ electrons at the transition. Indeed, our result for the local susceptibility shows itinerant-moment-like behavior, similar to that of the highly-pressurized $P\bar{1}$ phase (see Fig. 4). The $Pbnm$ phase is found to be metallic for all studied here unit cell volumes, as well as even for a large Hubbard $U = 12$ eV. The pressure-induced MIT is found to be accompanied by a collapse of the lattice volume by $\sim 5.2\%$, resulting in the melting of charge disproportionation of the Bi sites. Thus, in the $Pbnm$ phase all the Bi sites are equivalent, whereas the Bi $6s$ states are fully occupied, i.e., Bi^{3+}. Moreover, our analysis of eigenvalues of the reduced Ni $3d$ density matrix suggests that the Ni sites are in a Ni^{2+} state, with an atomic configuration $\simeq \sqrt{0.56}|d^8\rangle + \sqrt{0.30}|d^9\rangle$. We also notice a minor, below $\sim$10%, contribution due to the d^7 atomic state, $\sqrt{0.09}|d^7\rangle$. Based on this result, we conclude that no change of the valence state of the Ni^{2+} ions occurs across the pressure-induced MIT in $BiNiO_3$, i.e., the Ni^{2+} state remains stable. The latter is in a sharp contrast with the valence skipping Bi/Ni model proposed earlier for $BiNiO_3$ [11, 20]. Our results suggest a novel microscopic mechanism of a Mott MIT under pressure which is controlled by a charge-transfer between the A-site Bi $6s$ and ligand O $2p$ states. The pressure-induced MIT in $BiNiO_3$ is accompanied by a transition from the charge-disproportionated $\text{Bi1}^{3+}_{0.5}(\text{Bi2}^{(3+\delta)+}\underline{L}^{2-\delta})_{0.5}$ to the charge-uniform $Bi^{3+}\underline{L}^2$ valence state. The Bi $6s$ charge disproportionation (in the insulating $P\bar{1}$ phase) occurs together with the MIT, which follows rather than produces the structural transition. We therefore conclude that the pressure-induced MIT and the concomitant melting of the Bi $6s$ charge ordering in $BiNiO_3$ is driven by the crystal structure transition. The latter highlights the complex interplay between the electronic structure and lattice effects in the vicinity of a Mott MIT in RNiO$_3$ nickelates [3].

In conclusion, we employed the DFT+DMFT approach to determine the electronic structure and phase stability of paramagnetic $BiNiO_3$ across the pressure-induced Mott MIT. Our results for the $P\bar{1}$-structured $BiNiO_3$ under pressure propose a new mechanism for a correlation-driven metal-insulator transition, in which the Mott insulating state is (in much respect) controlled by the s-p level splitting between the uncorrelated A-site Bi $6s$ and ligand O $2p$ states. We show that the pressure-induced MIT in $BiNiO_3$ is associated with the melting of charge disproportionation of the Bi ions and is accompanied by delocalization of the Ni $3d$ electrons. The phase transition results in a charge transfer between the Bi $6s$ and O $2p$ states, while the Ni sites remain to be Ni^{2+}. Our results suggest that the pressure-induced change of the crystal structure drives the MIT in $BiNiO_3$. We argue that the RNiO$_3$ compounds (with R =rare earth and Bi) obey an intrinsic instability driven by the interplay of electron correlations and lattice effects, depending on the R-ion radius. It is associated with a crossover from charge disproportionation of the perovskite B-site Ni-ions (realized for the R-ions with the ionic radii smaller

than that of La) to that of the A-site R-ions (for large R-ions), with $LaNiO_3$ being in between.

We thank O. Peil for valuable discussions. We acknowledge the support from Russian Foundation for Basic Research (Project No. 18-32-20076).The DFT calculations were supported by the Ministry of Science and Higher Education of the Russian Federation (theme Electron No. AAAA-A18- 118020190098-5).

[1] M. Imada, A. Fujimori, Y. Tokura, Rev. Mod. Phys. **70**, 1039 (1998).

[2] S. Middey, J. Chakhalian, P. Mahadevan, J.W. Freeland, A.J. Millis, and D.D. Sarma, Annu. Rev. Mater. Res. **46**, 305 (2016); S. Catalano, M. Gibert, J. Fowlie, J. Íñiguez, J.-M. Triscone, and J. Kreisel, Rep. Prog. Phys. **81**, 46501 (2018).

[3] A. Subedi, O. E. Peil, and A. Georges, Phys. Rev. B **91**, 075128 (2015); A. B. Georgescu, O. E. Peil, A. S. Disa, A. Georges, and A. J. Millis, PNAS **116**, 14434 (2019); O. E. Peil, A. Hampel, C. Ederer, and A. Georges, Phys. Rev. B **99**, 245127 (2019).

[4] A. Mercy, J. Bieder, J. Íñiguez, and Ph. Ghosez, Nat. Commun. **8**, 1677 (2017).

[5] J. B. Torrance, P. Lacorre, A. I. Nazzal, E. J. Ansaldo, and Ch. Niedermayer, Phys. Rev. B **45**, 8209(R) (1992); J. L. García-Muñoz, J. Rodríguez-Carvajal, P. Lacorre, J. B. Torrance, Phys. Rev. B **46**, 4414 (1992); J. A. Alonso, J. L. García-Muñoz, M. T. Fernández-Díaz, M. A. G. Aranda, M. J. Martínez-Lope, M. T. Casais, Phys. Rev. Lett. **82**, 3871 (1999); G. Catalan, Phase Transit. **81**, 729 (2008); J. L. García-Muñoz, M. A. G. Aranda, J. A. Alonso, and M. J. Martínez-Lope, Phys. Rev. B **79**, 134432 (2009).

[6] M. Medarde, C. Dallera, M. Grioni, B. Delley, F. Vernay, J. Mesot, M. Sikora, J. A. Alonso, M. J. Martínez-Lope, Phys. Rev. B **80**, 245105 (2009).

[7] H. Park, A. J. Millis, and C. A. Marianetti, Phys. Rev. Lett. **109**, 156402 (2012); H. Park, A. J. Millis, and C. A. Marianetti, Phys. Rev. B **89**, 245133 (2014); **90**, 235103 (2014); A. Hampel and C. Ederer, *ibid.* **96**, 165130 (2017); A. Hampel, P. Liu, C. Franchini, and C. Ederer, npj Quant. Mater. **4**, 5 (2019).

[8] S. Johnston, A. Mukherjee, I. Elfimov, M. Berciu, and G. A. Sawatzky, Phys. Rev. Lett. **112**, 106404 (2014); J. Varignon, M. N. Grisolia, J. Íñiguez, A. Barthélémy, M. Bibes, npj Quant. Mater. **2**, 21 (2017).

[9] E. A. Nowadnick, J. P. Ruf, H. Park, P. D. C. King, D. G. Schlom, K. M. Shen, and A. J. Millis, Phys. Rev. B **92**, 245109 (2015).

[10] S. Ishiwata, M. Azuma, M. Takano, E. Nishibori, M. Takata, M. Sakatac, and K. Kato, J. Mater. Chem. **12**, 3733 (2002).

[11] M. Azuma, S. Carlsson, J. Rodgers, M. G. Tucker, M. Tsujimoto, S. Ishiwata, S. Isoda, Y. Shimakawa, M. Takano, and J. P. Attfield, J. Am. Chem. Soc. **129**, 14433 (2007).

[12] S. J. E. Carlsson, M. Azuma, Y. Shimakawa, M. Takano, A. Hewat, J. P. Attfield, J. Solid State Chem. **181**, 611 (2008).

[13] M. Azuma, W. Chen, H. Seki, M. Czapski, O. Smirnova, O. Kengo, M. Mizumaki, T. Watanuki, N. Ishimatsu, N. Kawamura *et al.*, Nat. Commun. **2**, 347 (2011); K. Oka, M. Mizumaki, Ch. Sakaguchi, A. Sinclair, C. Ritter, J. P. Attfield, and M. Azuma, Phys. Rev. B **88**, 014112 (2013).

[14] See Supplemental Material for a detailed discussion of the electronic structure and lattice properties of $BiNiO_3$ near the MIT.

[15] K. Momma and F. Izumi, J. Appl. Crystallogr. **44**, 1272 (2011).

[16] Interestingly, the insulating RNiO$_3$ phases also exhibit a complex (non-collinear) antiferromagnetic order below T_N, but with an uncommon wave vector $\mathbf{q} = (\frac{1}{2}, 0, \frac{1}{2})$.

[17] It is also interesting to point out that magnetic ordering is present only in the insulating triclinic phase. The metallic orthorhombic phase was found to be nonmagnetic down to 10 K [13].

[18] S. Ishiwata, M. Azuma, M. Hanawa, Y. Moritomo, Y. Ohishi, K. Kato, M. Takata, E. Nishibori, M. Sakata, I. Terasaki *et al.*, Phys. Rev. B **72**, 045104 (2005).

[19] H. Wadati, M. Takizawa, T. T. Tran, K. Tanaka, T. Mizokawa, A. Fujimori, A. Chikamatsu, H. Kumigashira, M. Oshima, S. Ishiwata *et al.*, Phys. Rev. B **72**, 155103 (2005).

[20] M. Mizumaki, N. Ishimatsu, N. Kawamura, M. Azuma, Y. Shimakawa, M. Takano, and T. Uozumi, Phys. Rev. B **80**, 233104 (2009).

[21] V. I. Anisimov, J. Zaanen, and O. K. Andersen, Phys. Rev. B **44**, 943 (1991).

[22] W. Metzner and D. Vollhardt, Phys. Rev. Lett. **62**, 324 (1989); A. Georges, G. Kotliar, W. Krauth, and M. J. Rozenberg, Rev. Mod. Phys. **68**, 13 (1996); V. I. Anisimov, A. I. Poteryaev, M. A. Korotin, A. O. Anokhin, and G. Kotliar, J. Phys. Condens. Matter **9**, 7359 (1997); G. Kotliar, S. Y. Savrasov, K. Haule, V. S. Oudovenko, O. Parcollet, and C. A. Marianetti, Rev. Mod. Phys. **78**, 865 (2006); J. Kuneš, I. Leonov, P. Augustinský, V. Křápek, M. Kollar, and D. Vollhardt, Eur. Phys. J. Special Topics **226**, 2641 (2017).

[23] M. Q. Cai, G. W. Yang, X. Tan, Y. L. Cao, L. L. Wang, W. Y. Hu, and Y. G. Wang, Appl. Phys. Lett. **91**, 101901 (2007); J. A. McLeod, Z. V. Pchelkina, L. D. Finkelstein, E. Z. Kurmaev, R. G. Wilks, A. Moewes, I. V. Solovyev, A. A. Belik, and E. Takayama-Muromachi, Phys. Rev. B **81**, 144103 (2010); S. Kojima, J. Nasu, and A. Koga, *ibid.* **94**, 045103 (2016); M. Naka, H. Seo, and Y. Motome, Phys. Rev. Lett. **116**, 056402 (2016); M. Pugaczowa-Michalska, J. Kaczkowski, Comp. Mater. Sci. **126**, 407 (2017); Y. Liu, Z. Wang, D. Chang, Q. Sun, M. Chao, Y. Jia, Comp. Mater. Sci. **113**, 198 (2016).

[24] A. Paul, A. Mukherjee, I. Dasgupta, A. Paramekanti, and T. Saha-Dasgupta, Phys. Rev. Lett. **122**, 016404 (2019).

[25] K. Haule, Phys. Rev. B **75**, 155113 (2007); L. V. Pourovskii, B. Amadon, S. Biermann, and A. Georges, *ibid.* **76**, 235101 (2007); B. Amadon, F. Lechermann, A. Georges, F. Jollet, T. O. Wehling, and A. I. Lichtenstein, *ibid.* **77**, 205112 (2008); M. Aichhorn, L. Pourovskii, V. Vildosola, M. Ferrero, O. Parcollet, T. Miyake, A. Georges, and S. Biermann, *ibid.* **80**, 085101 (2009).

[26] S. Baroni, S. de Gironcoli, A. Dal Corso, and P. Gian-

nozzi, Rev. Mod. Phys. **73**, 515 (2001); P. Giannozzi, S. Baroni, N. Bonini, M. Calandra, R. Car, C. Cavazzoni, D. Ceresoli, G. L. Chiarotti, M. Cococcioni, I. Dabo *et al.*, J. Phys.: Condens. Matter **21**, 395502 (2009).

[27] I. Leonov, N. Binggeli, Dm. Korotin, V. I. Anisimov, N. Stojić, and D. Vollhardt, Phys. Rev. Lett. **101**, 096405 (2008); I. Leonov, Dm. Korotin, N. Binggeli, V. I. Anisimov, and D. Vollhardt, Phys. Rev. B **81**, 075109 (2010).

[28] M. Aichhorn, S. Biermann, T. Miyake, A. Georges, and M. Imada, Phys. Rev. B **82**, 064504 (2010); O. E. Peil, A. Georges, and F. Lechermann, Phys. Rev. Lett. **107**, 236404 (2011); K. Ohta, R. E. Cohen, K. Hirose, K. Haule, K. Shimizu, and Y. Ohishi, Phys. Rev. Lett. **108**, 026403 (2012); D. Grieger, Ch. Piefke, O. E. Peil, and F. Lechermann, Phys. Rev. B **86**, 155121 (2012); I. Leonov, V. I. Anisimov, and D. Vollhardt, *ibid.* **91**, 195115 (2015); I. Leonov, *ibid.* **92**, 085142 (2015); A. O. Shorikov, A. V. Lukoyanov, V. I. Anisimov, and S. Y. Savrasov, *ibid.* **92**, 035125 (2015); I. Leonov, S. L. Skornyakov, V. I. Anisimov, and D. Vollhardt Phys. Rev. Lett. **115**, 106402 (2015); I. Leonov, L. Pourovskii, A. Georges, and I. A. Abrikosov, Phys. Rev. B **94**, 155135 (2016); F. Lechermann, N. Bernstein, I. I. Mazin, and R. Valenti, Phys. Rev. Lett. **121**, 106401 (2018); E. Greenberg, I. Leonov, S. Layek, Z. Konopkova, M. P. Pasternak, L. Dubrovinsky, R. Jeanloz, I. A. Abrikosov, and G. Kh. Rozenberg, Phys. Rev. X **8**, 031059 (2018); I. Leonov, G. Kh. Rozenberg, and I. A. Abrikosov, npj Comput. Mater. **5**, 90 (2019).

[29] N. Marzari, A. A. Mostofi, J. R. Yates, I. Souza, and D. Vanderbilt, Rev. Mod. Phys. **84**, 1419 (2012); V. I. Anisimov, D. E. Kondakov, A. V. Kozhevnikov, I. A. Nekrasov, Z. V. Pchelkina, J. W. Allen, S.-K. Mo, H.-D. Kim, P. Metcalf, S. Suga *et al.*, Phys. Rev. B **71**, 125119 (2005); Dm. Korotin, A. V. Kozhevnikov, S. L. Skornyakov, I. Leonov, N. Binggeli, V. I. Anisimov, and G. Trimarchi, Eur. Phys. J. B **65**, 91 (2008); G. Trimarchi, I. Leonov, N. Binggeli, Dm. Korotin, and V. I. Anisimov, J. Phys.: Condens. Matter **20**, 135227 (2008).

[30] E. Gull, A. J. Millis, A. I. Lichtenstein, A. N. Rubtsov, M. Troyer, and P. Werner, Rev. Mod. Phys. **83**, 349 (2011).

[31] J. Zaanen, G. A. Sawatzky, and J. W. Allen, Phys. Rev. Lett. **55**, 418 (1985); M. A. Korotin, V. I. Anisimov, D. I. Khomskii, and G. A. Sawatzky Phys. Rev. Lett. **80**, 4305 (1998).

[32] F. C. Zhang and T. M. Rice, Phys. Rev. B **37**, 3759(R) (1988).

[33] J. P. Wright, J. P. Attfield, and P. G. Radaelli, Phys. Rev. B **66**, 214422 (2002); I. Leonov, A. N. Yaresko, V. N. Antonov, and V. I. Anisimov, *ibid.* **74**, 165117 (2006); H.-T. Jeng, G. Y. Guo, and D. J. Huang, *ibid.* **74**, 195115 (2006); M. S. Senn, J. P. Wright, and J. P. Attfield, Nature **481**, 173 (2012); N. Pontius, T. Kachel, C. Schüßler-Langeheine, W. F. Schlotter, M. Beye, F. Sorgenfrei, C. F. Chang, A. Föhlisch, W. Wurth, P. Metcalf *et al.*, Appl. Phys. Lett. **98**, 182504 (2011); G. Perversi, E. Pachoud, J. Cumby, J. M. Hudspeth, J. P. Wright, S. A. J. Kimber, J. P. Attfield, Nat. Commun. **10**, 2857 (2019).

[34] K. Foyevtsova, A. Khazraie, I. Elfimov, and G. A. Sawatzky, Phys. Rev. B **91**, 121114(R) (2015); N. C. Plumb, D. J. Gawryluk, Y. Wang, Z. Ristić, J. Park, B. Q. Lv, Z. Wang, C. E. Matt, N. Xu, T. Shang *et al.*, Phys. Rev. Lett. **117**, 037002 (2016); A. Khazraie, K. Foyevtsova, I. Elfimov, and G. A. Sawatzky Phys. Rev. B **98**, 205104 (2018).

[35] The crystal field levels for the Ni e_g states taken here as a reference energy are evaluated from the first moments of the interacting lattice Green's function as $\Delta_{\rm cf} \equiv {\rm diag}[\Sigma_{\mathbf{k}} H^{\rm DFT}(\mathbf{k}) + {\rm Re}\Sigma(i\omega_n \to \infty)]$. Here, $H^{\rm DFT}(\mathbf{k})$ is the effective low-energy *s*-*p*-*d* Hamiltonian in the Wannier basis set. $\Sigma(i\omega_n \to \infty)$ is a static Hartree contribution from self-energy $\Sigma(i\omega_n)$.

Supplemental Material

Under ambient pressure, $BiNiO_3$ adopts a highly distorted perovskite (triclinic) crystal structure with space group $P\bar{1}$ (see Supplementary Fig. S1). It has two inequivalent Bi and four Ni sites and is characterized by the cooperative breathing Bi-O distortions of the lattice. The Bi sites are arranged in chains along the c axis, with a checkerboard pattern in the ab-plane. The $P\bar{1}$-structured $BiNiO_3$ is an insulator with an energy gap of ~ 0.68 eV as estimated from the electrical resistivity [1].

Under pressure above ~ 4 GPa, $BiNiO_3$ undergoes a structural transformation to the orthorhombic $GdFeO_3$-type ($Pbnm$) crystal structure, which has a single type of Bi and Ni ions. The phase transition is accompanied by a Mott insulator-to-metal transition and is associated with suppression of the breathing distortions of the lattice (all the Ni and Bi sites become equivalent in the $Pbnm$ phase).

Here, we employed the DFT+DMFT approach to explore the electronic properties and phase stability of paramagnetic $BiNiO_3$ under pressure using the DFT+DMFT method [2] implemented with plane-wave pseudopotentials [3, 4]. We start by constructing the effective low-energy Hamiltonian $[\hat{H}^{\rm DFT}_{\sigma,\alpha\beta}(\mathbf{k})]$, which explicitly contains the Bi $6s$, Ni $3d$, and O $2p$ valence states, using the projection onto Wannier functions [5]. For this purpose, for the partially filled Bi $6s$, Ni $3d$, and O $2p$ orbitals we construct a basis set of atomic-centered symmetry-constrained Wannier functions [6]. The Wannier functions are constructed over the full energy range spanned by the s-p-d band complex using the scheme of Ref. [6]. We obtain the s-p-d Hubbard Hamiltonian (in the density-density approximation)

$$\hat{H} = \sum_{\mathbf{k},\sigma} \hat{H}^{\rm DFT}_{\sigma,\alpha\beta}(\mathbf{k}) + \frac{1}{2} \sum_{i,\sigma\sigma',\alpha\beta} U^{\sigma\sigma'}_{\alpha\beta}\, \hat{n}_{i,\alpha\sigma}\hat{n}_{i,\beta\sigma'} - \hat{H}_{\rm DC},$$

where $\hat{n}_{i,\alpha\sigma}$ is the occupation number operator for the i-th Ni site with spin σ and (diagonal) orbital indices α. In Supplementary Fig. S2 we show our results for the band structure of $BiNiO_3$ calculated within nonmagnetic DFT in comparison with the Wannier Bi $6s$, Ni $3d$, and O $2p$ band structure for the ambient-pressure $P\bar{1}$ and high-pressure $Pbmn$ phases of $BiNiO_3$. Our results for the leading Wannier hopping integrals between the Bi $6s$ and neighbor ions in the ambient-pressure $P\bar{1}$ and high-pressure $Pbnm$ phases of $BiNiO_3$ are summarized in Table S1. All the calculations are performed in the local basis set determined by diagonalization of the corresponding Ni $3d$ occupation matrices.

In order to solve the realistic many-body problem, we employ the continuous-time hybridization-expansion quantum Monte-Carlo algorithm [7]. The Coulomb interaction has been treated in the density-density approximation. The elements of the U matrix are parametrized by the average Coulomb interaction U and Hund's exchange J for the Ni $3d$ shell. For all the structural phases considered here we have used the same $U = 6$ eV and $J = 0.95$ eV values as was estimated previously for RNiO$_3$ [8, 9]. The spin-orbit coupling was neglected in these calculations. Moreover, the U and J values are assumed to remain constant upon variation of the lattice volume. We employ the fully localized double-counting correction, evaluated from the self-consistently determined local occupations, to account for the electronic interactions already described by DFT, $\hat{H}_{DC} = U(N - \frac{1}{2}) - J(N_\sigma - \frac{1}{2})$, where N_σ is the total Ni $3d$ occupation with spin σ and $N = N_\uparrow + N_\downarrow$. Here, we employ a fully self-consistent in charge density DFT+DMFT scheme in order to take into account the effect of charge redistribution caused by electronic correlations and electron-lattice coupling.

In Supplementary Fig. S3 we show the spectral functions of paramagnetic $BiNiO_3$ calculated by DFT+DMFT in comparison with photoemission (PES) and X-ray absorption (XAS) spectra taken at room temperature [10]. Our calculations are performed in the paramagnetic state at a temperature $T = 387$ K, above the Néel temperature $T_{\rm N} \sim 300$ K. To calculate the spectral functions, we employ the Padé analytical continuation procedure for the self-energy. In our calculations we adopt the experimental crystal structure data (atomic positions for the orthorhombic phase are taken from the experiment at a pressure of $\sim$7.7 GPa [11]).

The calculated spectral functions are in overall good agreement with the experimental spectra. In particular, in the insulating triclinic phase, the energy gap lies between the occupied and unoccupied Ni e_g states, strongly mixed with the O $2p$ and the empty Bi2 $6s$ states (the Bi1 $6s$ states are fully occupied). Our results indicate that all the Ni sites (the insulating $P\bar{1}$ phase has four inequivalent Ni sites) are nearly equivalent. A sharp peak at about -1.5 eV originates from the occupied Ni t_{2g} states, which form a lower Hubbard band at -9 eV. The PES spectral weight lying at about -3 and -5 eV is mainly due to the O $2p$ states, the hump at -10 eV is predominantly due to the Bi $6s$ states. In the metallic orthorhombic phase, the peak at the Fermi level and the spectral weight at the bottom of the conduction band are predominantly formed by the Ni e_g and O $2p$ states. The Ni e_g upper Hubbard band appears at ~ 1.0 eV. The peak at about -1.5 eV is due to the occupied Ni t_{2g} states. In contrast to the insulating phase, all the Bi states are occupied and are located at about -10 eV.

[1] S. Ishiwata, M. Azuma, M. Takano, E. Nishibori, M. Takata, M. Sakatac, and K. Kato, J. Mater. Chem. **12**, 3733 (2002).

TABLE S1: Leading Wannier hopping integrals (in meV) between Bi 6s and neighbor ions in the ambient-pressure $P\bar{1}$ (left part) and high-pressure $Pbnm$ (right part) phases of $BiNiO_3$.

Atom	Atom	Distance (a.u.)	Hoppings (meV)
Bi 6s	O 2p	4.08	-1304, -1234, -71
Bi 6s	O 2p	4.11	-1410, 1037, 631
Bi 6s	O 2p	4.48	-280, -404, 1086
Bi 6s	O 2p	4.62	772, 295, 1144
Bi 6s	O 2p	4.86	-674, 72, 839
Bi 6s	O 2p	4.90	422, 47, -916
Bi 6s	O 2p	5.41	052, -80, -757
Bi 6s	O 2p	5.98	-385, 78, 204
Bi 6s	Ni e_g	6.03	41, 2
Bi 6s	Ni t_{2g}	6.03	-37, 75, 163
Bi 6s	Ni e_g	6.10	-7, 58
Bi 6s	Ni t_{2g}	6.10	31, -126, -142
Bi 6s	Ni e_g	6.11	11, 48
Bi 6s	Ni t_{2g}	6.11	-2, -274, -163
Bi 6s	Ni e_g	6.16	40, 12
Bi 6s	Ni t_{2g}	6.16	58, -14, 64

Atom	Atom	Distance (a.u.)	Hoppings (meV)
Bi 6s	O 2p	4.24	0, 1709, 242
Bi 6s	O 2p	4.44	-271, -1536, 95
Bi 6s	O 2p	4.44	-271, -1536, -95
Bi 6s	O 2p	4.58	0, 622, 1132
Bi 6s	O 2p	4.85	-69, -103, 957
Bi 6s	O 2p	4.85	-69, -103, -957
Bi 6s	O 2p	4.95	6, -142, 935
Bi 6s	O 2p	4.95	6, -142, -935
Bi 6s	O 2p	5.85	0, -298, -151
Bi 6s	O 2p	5.85	0, -49, -330
Bi 6s	Ni e_g	5.86	-6, -11
Bi 6s	Ni t_{2g}	5.86	40, -12, 227
Bi 6s	Ni e_g	5.86	6, 11
Bi 6s	Ni t_{2g}	5.86	40, -12, 227
Bi 6s	Ni e_g	6.11	0, -40
Bi 6s	Ni t_{2g}	6.11	38, 156, -55

[2] K. Haule, Phys. Rev. B **75**, 155113 (2007); L. V. Pourovskii, B. Amadon, S. Biermann, and A. Georges, *ibid.* **76**, 235101 (2007); B. Amadon, F. Lechermann, A. Georges, F. Jollet, T. O. Wehling, and A. I. Lichtenstein, *ibid.* **77**, 205112 (2008); M. Aichhorn, L. Pourovskii, V. Vildosola, M. Ferrero, O. Parcollet, T. Miyake, A. Georges, and S. Biermann, *ibid.* **80**, 085101 (2009); M. Aichhorn, S. Biermann, T. Miyake, A. Georges, and M. Imada, Phys. Rev. B **82**, 064504 (2010); O. E. Peil, A. Georges, and F. Lechermann, Phys. Rev. Lett. **107**, 236404 (2011); D. Grieger, Ch. Piefke, O. E. Peil, and F. Lechermann, Phys. Rev. B **86**, 155121 (2012); I. Leonov, V. I. Anisimov, and D. Vollhardt, *ibid.* **91**, 195115 (2015).

[3] S. Baroni, S. de Gironcoli, A. Dal Corso, and P. Giannozzi, Rev. Mod. Phys. **73**, 515 (2001); P. Giannozzi, S. Baroni, N. Bonini, M. Calandra, R. Car, C. Cavazzoni, D. Ceresoli, G. L. Chiarotti, M. Cococcioni, I. Dabo *et al.*, J. Phys.: Condens. Matter **21**, 395502 (2009).

[4] I. Leonov, N. Binggeli, Dm. Korotin, V. I. Anisimov, N. Stojić, and D. Vollhardt, Phys. Rev. Lett. **101**, 096405 (2008); I. Leonov, Dm. Korotin, N. Binggeli, V. I. Anisimov, and D. Vollhardt, Phys. Rev. B **81**, 075109 (2010).

[5] N. Marzari, A. A. Mostofi, J. R. Yates, I. Souza, and D. Vanderbilt, Rev. Mod. Phys. **84**, 1419 (2012).

[6] V. I. Anisimov, D. E. Kondakov, A. V. Kozhevnikov, I. A. Nekrasov, Z. V. Pchelkina, J. W. Allen, S.-K. Mo, H.-D. Kim, P. Metcalf, S. Suga *et al.*, Phys. Rev. B **71**, 125119 (2005); Dm. Korotin, A. V. Kozhevnikov, S. L. Skornyakov, I. Leonov, N. Binggeli, V. I. Anisimov, and G. Trimarchi, Eur. Phys. J. B **65**, 91 (2008); G. Trimarchi, I. Leonov, N. Binggeli, Dm. Korotin, and V. I. Anisimov, J. Phys.: Condens. Matter **20**, 135227 (2008).

[7] E. Gull, A. J. Millis, A. I. Lichtenstein, A. N. Rubtsov, M. Troyer, and P. Werner, Rev. Mod. Phys. **83**, 349 (2011).

[8] H. Park, A. J. Millis, and C. A. Marianetti, Phys. Rev. Lett. **109**, 156402 (2012); H. Park, A. J. Millis, and C. A. Marianetti, Phys. Rev. B **89**, 245133 (2014); H. Park, A. J. Millis, and Ch. A. Marianetti, Phys. Rev. B **90**, 235103 (2014).

[9] E. A. Nowadnick, J. P. Ruf, H. Park, P. D. C. King, D. G. Schlom, K. M. Shen, and A. J. Millis, Phys. Rev. B **92**, 245109 (2015).

[10] H. Wadati, M. Takizawa, T. T. Tran, K. Tanaka, T. Mizokawa, A. Fujimori, A. Chikamatsu, H. Kumigashira, M. Oshima, S. Ishiwata *et al.*, Phys. Rev. B **72**, 155103 (2005).

[11] M. Azuma, S. Carlsson, J. Rodgers, M. G. Tucker, M. Tsujimoto, S. Ishiwata, S. Isoda, Y. Shimakawa, M. Takano, and J. P. Attfield, J. Am. Chem. Soc. **129**, 14433 (2007).

[12] K. Momma and F. Izumi, J. Appl. Crystallogr. **44**, 1272 (2011).

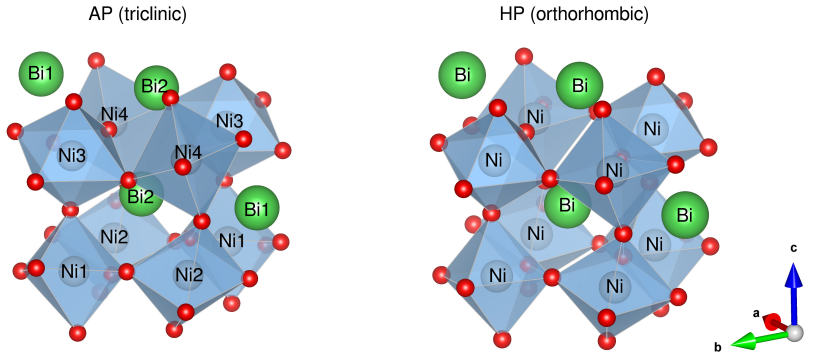

FIG. S1: (Color online) Crystal structure of the triclinic $P\bar{1}$ (left) and highly-pressurized orthorhombic $Pbnm$ (right) phases of $BiNiO_3$. The oxygen atoms are depicted by small red balls. The figure was prepared with the VESTA program [12].

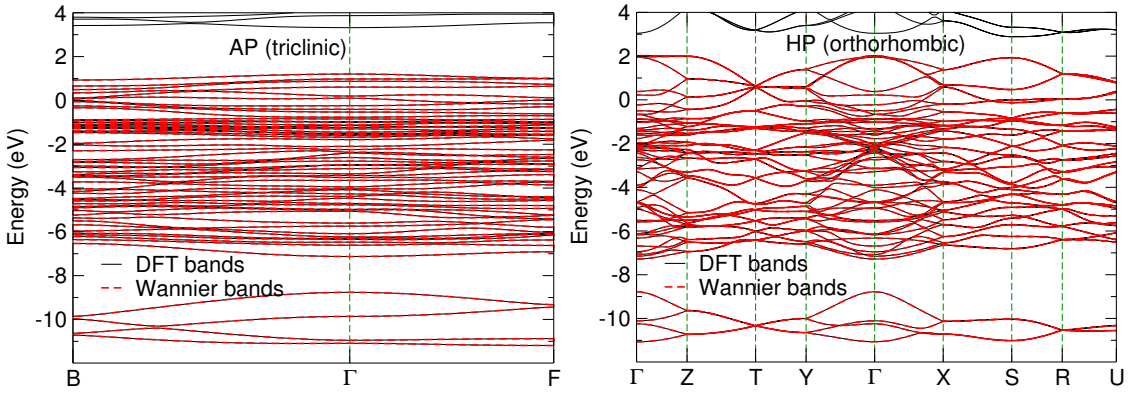

FIG. S2: (Color online). Band structure of $BiNiO_3$ calculated within nonmagnetic DFT for the ambient-pressure $P\bar{1}$ (left panel) and high-pressure $Pbnm$ (right panel) phases in comparison with the Wannier bands corresponding to the constructed Bi $6s$, Ni $3d$, and O $2p$ Wannier functions (red dashed lines). The Fermi level is at zero energy.

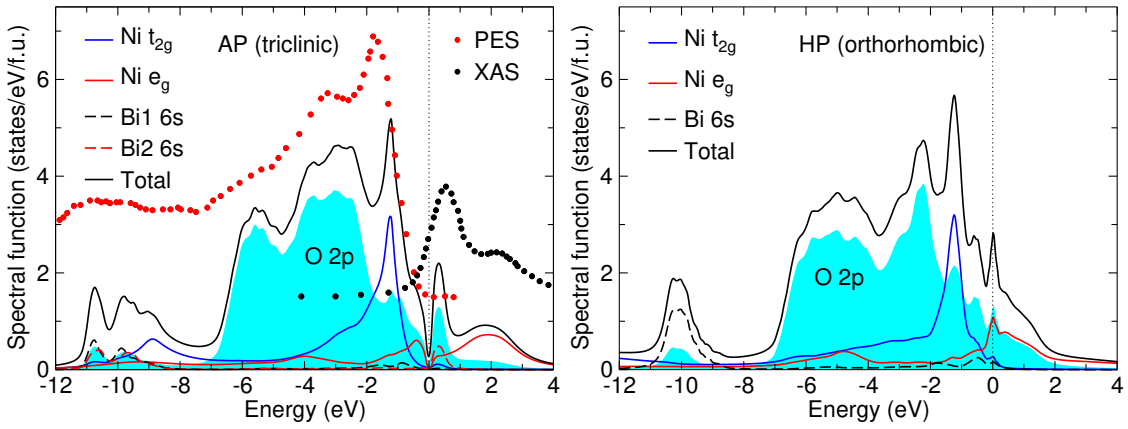

FIG. S3: (Color online). Orbitally-resolved spectral functions of paramagnetic $BiNiO_3$ calculated within DFT+DMFT for the ambient-pressure $P\bar{1}$ (left panel) and high-pressure $Pbnm$ (right panel) phases of $BiNiO_3$. Photoemission (PES) and X-ray absorption (XAS) spectra are shown for comparison [10]. The DFT+DMFT calculations are performed at a temperature $T = 387$ K (above $T_N \sim 300$ K). The Fermi level is at zero energy.